

Theoretical and Experimental Investigation on Microcosmic Surface Generation in Precision Grinding with Discrete Method

Yizun Chen[1] – Yu Sun[2] ✉

[1] Xi'an University of Architecture and Technology, School of Building Services Science and Engineering, China
[2] Xi'an University of Architecture and Technology, School of Science, China
✉ sunlyu@xauat.edu.cn

Abstract *Surface topography of the workpiece created in precision grinding is influenced by not only key process parameters, but also the distribution characteristics of active abrasive grits on the surface of the grinding wheel, including the number of active grits in the contact zone, the morphology of grits, and the cutting depth of a single grit in a normal direction. Under the conditions of small cutting depth (less than 5 μm) with small eccentrical rotation of the abrasive wheel (less than 3 μm), the influences of the original workpiece surface topography characteristics and the dynamic cutting depth of abrasive grits are often neglected in the study of microcosmic surface generation. In this paper, a discrete method (DM) is used to develop a theoretical kinematics model for the prediction of machined workpiece surface topography. Compared with the characteristics value of surface topography (scratch grooves) between experimental measurement and simulation output, the verification results from the improved prediction model of surface topography present well in comprehensively considering the influences of original surface characteristics, eccentrically rotational behavior of the abrasive wheel and the overlapped situation of scratch grooves on complex process conditions with a prediction error of about 10 %. In comparison with two commonly used empirical formulas in many other research studies, the prediction accuracy of the DM model for machined surface topography improves by 20 %. When calculating material removal volume, the prediction accuracy of incremental volume model of material removal increases approximately by 9 % to 19 % in comparison with the prediction results that take the whole cross-section area of an active grit as a key variable.*

Keywords *precision grinding, microcosmic surface topography, depth of cut, discrete method (DM), surface roughness*

Highlights

- *Presented improved kinematics model considering original surface, wheel eccentricity, and groove overlap.*
- *A discrete method (DM) is used to develop the enhanced kinematics model of surface topography.*
- *DM model improved topography prediction accuracy by 20 % compared to common empirical formulas.*
- *Material removal model accuracy improved by 9 % to 19 % compared to full cross-section-based predictions.*

1 INTRODUCTION

Precision surface grinding is one of the primary processes to acquire surface finish of the metal workpieces in high accuracy. In the process, slender and thin chips are removed from the workpiece surface by continuously working abrasive grits distributed on the surface of the grinding wheel that is installed on the machine tool spindle. The results demonstrate that surface accuracy of the machined workpiece is comprehensively influenced by linear and nonlinear factors, including process parameters, preparation and dressing/truing conditions of abrasive wheel, mechanical properties of the workpiece material, and the thermal-mechanical coupling relationship during grinding [1-4]. As one of the main surface topography characteristics in evaluating machining accuracy, surface roughness of the workpiece is closely relevant to the distribution characteristics of active abrasive grits on the surface of the wheel in axial and peripheral directions, such as the number of active grits in the contact zone, morphology combination of the grits, and cutting depth or moving trajectory path of each grit in a normal direction, etc. [5-6].

There are two types of relatively mature techniques currently utilized for predicting and evaluating surface accuracy of the machined workpiece. By means of different prediction models or digital fitting methods with some process parameters, the first technique is to establish an empirical formula for predicting the surface topography of the workpiece by considering a high correlation between the characteristic data of surface topography as measured by experiments and specific process parameters. Based on a material removal mechanism, the other technique is to develop a theoretical model of the workpiece surface topography and further to conduct the numerical solutions of surface topography characteristics in high precision. The validity of both techniques mentioned above is verified by results from the corresponding experiments.

By utilizing the first technique, Zagórski et al. [7], Li et al. [8] and Wang et al. [9] presented a prediction model using artificial neural networks and a logarithmic or exponential correlation model between surface roughness of the machined workpiece and some process parameters, including substrate size or grinding radius of the abrasive wheel, particle size and hardness of the grits, total cutting depth, rotatory speed of abrasive wheel, feed rate of workpiece, etc., and further conducted surface topography prediction or surface quality evaluation. By evaluating how strongly different surface-generation process parameters affect the outcome, and validating the results against experimental measurements and simulated surface-roughness data, this method provides a straightforward way to build a surface-topography prediction model and to estimate the expected machining accuracy of a workpiece from the chosen process parameters.. For example, numerous nonlinear influential factors are often

 DOI: 10.5545/sv-jme.2025.1386

neglected regarding surface generation under conditions of small cutting depth (less than 5 µm). In addition to process parameters, machining accuracy is also affected by the mechanical properties of the workpiece material, grinding performance and distribution characteristic of active grits in the contact zone [1-3,6], and dressing/truing/wear conditions of the abrasive wheel [5], etc. Therefore, the prediction accuracy of proposed empirical models may be limited by a lack of consideration of how the aforementioned nonlinear influential factors work on surface generation.

The grinding process is a cutting operation in which abrasive grits grind the workpiece material into the desired surface topography. Under the condition of cutting depth of a single abrasive grit in the range of a micrometer, the material removal mechanism of precision surface grinding involves slender chips of the workpiece material being gradually removed by means of continuously active abrasive grits randomly or orderly distributed on the surface of the rotating abrasive wheel. Then a microcosmic surface generation of the workpiece at a much finer scale is achieved by means of various scratch grooves formation processes along the axial direction of abrasive wheel (i.e. the direction of measuring surface roughness). By adopting the second technique based on this mechanism, many researchers systematically studied material removal behavior in the feed direction of the workpiece and then proposed theoretical models of the microcosmic surface topography of the workpiece, using cutting depth and trajectory path of abrasive grits in one dimension or two dimensions to predict surface roughness and machining accuracy. As this technique mainly depends on the material removal mechanism, the presented models of surface topography and their application have better adaptability in higher prediction accuracy than those derived from the first technique. Zhang et al. [1] proposed a theoretical model based on average protrusion heights of abrasive grits arranged in an orderly way on the surface of the abrasive wheel and further presented the theoretical model of surface topography of the workpiece machined in a trajectory direction along which the workpiece material was removed. Zhu et al. [10] proposed an improved model of surface topography by comprehensively considering process parameters, including particle size and number of abrasive grits and their distribution characteristics around the circumference of the abrasive wheel. Santhosh et al. [11] and Zou et al. [12] proposed mathematical models of surface topography based on a generation mechanism of the maximum undeformed chip of material removed by abrasive grits as randomly distributed on the surface of the abrasive wheel. Rasim et al. [3] and Duan et al. [13] studied the removal process of brittle material exerted by single and multiple abrasive grits based on the assumption that all geometries of abrasive grits were uniform in morphology, and then analyzed surface generation of the workpiece by means of scratching experiments using abrasive grits. Axinte et al. [6] and Hu et al. [14] predicted surface topography and machining accuracy with a dynamic's simulation method of the grinding process by comprehensively considering the geometry combinations of abrasive grits in shapes of spherical, conical with rounded corner and cube. Guo et al. [15] proposed prediction and evaluation models of three-dimensional surface topography in microscale based on molecular dynamics theory. Zagórski et al. [16] and Jia et al. [17] developed prediction models of surface topography on conditions of rough milling magnesium alloy and grinding ceramic materials by using tools with different geometries.

The eccentrically rotational behavior of an abrasive wheel is seldom considered as one of the influential factors on surface generation in most theoretical models of surface topography based on material removal mechanism, especially under the condition of micro-grinding. The behavior involves material being removed by many abrasive grits on the surface of an abrasive wheel eccentrically rotating with uneven radius around the center of a machine tool spindle in which assembly error between machine tool spindle and abrasive wheel spindle results in dynamic wear of the abrasive wheel. This wear results in a wavy surface on the workpiece, which can be measured in axial and peripheral directions. Likewise, the influence of original surface characteristics (such as micro-unevenness of surface) of the workpiece on actual cutting depth or material removal rate is also neglected or insufficiently considered in most scientific research. The situation presumes that a preset total cutting depth is removed from a workpiece with an "absolutely horizontal" surface with no waviness, which obviously does not conform to the actual situation. Accordingly, the influential mechanism of corresponding material removal increment between the original surface characteristics and instantaneous cutting depth per rotation of adjacent abrasive grits on surface generation is not fully revealed.

In this paper, quantitative characterization and restructuration considering the original surface topography of the workpiece are conducted by exerting a discrete method (DM) considering characteristic values of a wavy surface (e.g., peak and valley of surface waviness) as measured in experiments. The comprehensive influence of original surface characteristics and eccentrically rotational behavior of an abrasive wheel on microcosmic surface generation is studied and further, the theoretical models of instantaneous cutting depth of continuously working abrasive grits in a contact zone and incremental removal volume of material are presented. The validity and reliability of the models are verified by comparing them with the prediction outputs of the improved model and experimental results of the surface topography in axial and peripheral directions.

2 METHODS AND MATERIALS

2.1 Theoretical Model of Grinding Kinematics

The theoretical model of grinding kinematics or dynamics is illustrated in Fig. 1a. Here X, Y and Z axes represent the normal direction of the abrasive wheel, feed direction of the workpiece, and axial direction of the abrasive wheel respectively. In most research, it is assumed that the rotatory center of abrasive wheel coincides with the installation center of the machine tool spindle, which implies that the influence of eccentrically rotational movement of the abrasive wheel on material removal and the workpiece surface generation is neglected. As shown in the enlarged and three-dimensional (3D) diagram of Fig. 1b, the moving active abrasive grits in different geometries with varied protrusion heights remove materials from the workpiece, which results in microcosmic surface generation of the workpiece in shapes of many slim scratches (grooves) staggered or overlapped with a certain spatial distance. The cross-sectional characteristics (e.g., cutting depth $h_r(\varphi_i)$, contact length l_p and width B_i) of a single groove is represented in Fig. 1b (top-left view [6]). Various shapes and depths of grooves in some X-Z sectional plane of the workpiece surface (in green in Fig. 1b) are enlarged in Fig. 1c.

As shown in Fig. 1b, the workpiece surface during the grinding process is approximately composed of three parts, ie. machined surface, surface machining and surface to be machined. In the zone of machined surface, microcosmic surface topography with staggered or overlapped grooves in X–Z cross-sectional plane (in green) along the direction of the measuring surface roughness (in red) has been generated by working abrasive grits consecutively [1]. In one X–Z sectional plane in Fig. 1c, the mathematical model of surface roughness is characterized by extracting workpiece surface feature values of peak-points (v_1–v_n) and valley-points (w_1–w_n) obtained from experiments, and is used to evaluate the machining accuracy.

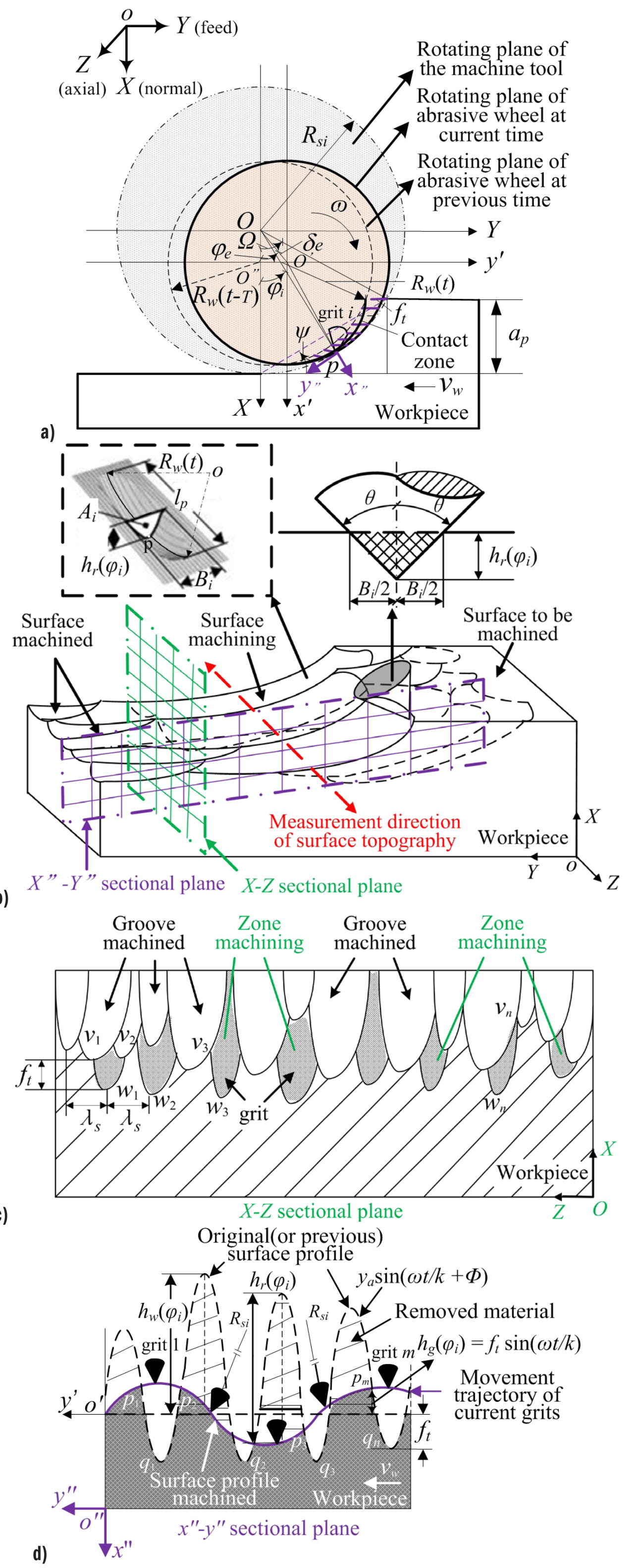

Fig. 1. Improved kinematics model and material removal model under condition of eccentrically rotating of wheel in a precision grinding process; a) kinematics model of precision grinding; b) the 3D surface topography processed by continuous abrasive grits and single groove by an abrasive grit; c) the microcosmic surface topography processed by continuous abrasive grits in one $X-Z$ sectional plane; and d) the microcosmic surface topography processed by continuous abrasive grits in one $X''-Z''$ sectional plane

In Figure 1c, the wavy surface generation and the features of surface roughness are mainly affected by key process parameters, including total cutting depth and rotating speed ratio of the workpiece and the abrasive wheel, etc, when large cutting depths of over 10 µm are adopted. It means that the effect of grit morphology and eccentric rotational behavior of the grinding wheel on the characteristics value of surface topography is not crucial in the situation. However, the situation becomes different when the cutting depth is less than 5 µm or even less than 1 µm (i.e. approximately one order of magnitude to the eccentricity value of abrasive wheel) in precision or ultra precision grinding. Set a temporary reference coordinate system $o''-x''-y''$ on a cutting point p in a peripheral direction when a single grit is scratching, as shown in contact zone in Fig. 1a. Here x''-axial and y''-axial represent normal and peripheral directions related to a single active grit on the surface of the abrasive wheel respectively. It is assumed that the number of active abrasive grits with various morphology geometries (e.g., conical, cuboid and sphere, etc. [2,3]) working simultanuously in a grit-workpiece interaction zone (i.e. grinding contact zone) is m. Influenced by the excitation of eccentric rotational behavior of the abrasive wheel, the characteristic values of peak-points (p_1-p_n) and valley- points (q_1-q_n) extracted from the wavy surface in one $x''-y''$ peripheral sectional plane (in red-purple in Fig. 1b) are shown in Fig. 1d and are fully discretized after the workpiece material is removed by active grits rotating with a certain eccentricity radius. However, these peak- and valley- points in one peripheral-sectional plane in Fig. 1d could be interfered with or coincided by those also expressed with peak-points (v_1-v_n) and valley- points (w_1-w_n) in one normal-sectional plane shown in Fig. 1c. Thus microcosmic surface topography in normal- (Fig. 1c) and peripheral- (Fig. 1d) sectional planes have close relations with the grit morphology characteristics and present the material removing capability of active abrasive grits. For example, the size, placement, shape and cutting depth of active grits in the normal direction are crucial to the length, width, depth, peak-points and valley-points of scratch grooves on the surface of the workpiece and their overlapping situation. The three-dimensional surface topography of the machined workpiece and its characteristics, such as surface waviness and surface roughness are determined by not only the characteristic values of peak-valley points on the workpiece surface in the $X-Z$ normal-sectional plane, but also the maximum values of characteristics both in the $X-Z$ normal-sectional plane and in the $X''-Y''$ peripheral-sectional plane. The aforementioned theories provide the main principles for developing an improved theoretical model of microcosmic surface topography and conducting data discretization in the research.

2.2 Theoretical Model of Eccentrically Rotational Behavior of Abrasive Wheel

During the actual grinding process, the initial error is generated by the unavoidable eccentric installation of the abrasive wheel, which results in nonuniform material removal from the workpiece. As shown in Fig. 1a, an abrasive wheel of substrate radius R_w is installed on the rotatory center O' and rotates with angular speed ω (or peripheral speed v_s). The workpiece moves forwards with feed speed v_w and the material is removed at the same peak position p and in time interval T with instantaneous and incremental cutting depth $h_r(\varphi_i)$ in the normal direction by adjacent abrasive grits in which the rotatory radii are $R_w(t)$ and $R_w(t-T)$ at the instant time t and previous time $t-T$ respectively. Microcosmic surface with a certain waviness in one normal-section plane (i.e. $X-O-Z$ plane) is generated after the material is removed, as illustrated in machining zone in Fig. 1c. As shown in the enlarged Fig. 1d, the material is removed with an incremental cutting depth of $h_r(\varphi_i)$ by eccentrically rotating grits in one peripheral section plane (i.e. $X''-O''-Y''$ plane), and the wavy surface whose characteristics marked with peak-points ($p_1 - p_n$) and valley-points ($q_1 - q_n$), respectively, is obtained.

In Fig. 1a, the variable $\delta_e = \overline{OO'}$ is defined as error derived from the eccentric installation of the abrasive wheel, which increases with deterioration from dynamic wear of the wheel during grinding. The value of the eccentric error is limited at the range of 1 µm to 3 µm to avoid the severe grinding chatter that significantly decreases the abrasive wheel life and results in defective products. When total cutting depth is a_p, the effective grinding radius R_{si} ($i = 1, 2, \ldots, m$) of a single abrasive grit i from the rotatory center O' to the cutting position p in contact zone is calculated as [18]:

$$R_{si} = R_w + \Lambda_{si} + \delta_e \cos\varphi_{e0i}, \tag{1}$$

where R_w is the radius of the abrasive wheel substrate; and Λ_{si} protrusion height of abrasive grit i from the surface of the wheel, which is a characteristic variable that conforms to the Gaussian distribution with the mean value Λ_{savg} and the standard deviation σ [1,9]. Variable φ_{e0i} is defined as the initial installation position angle of current grit i to rotatory center O', which is calculated according to the initial installation location of the abrasive wheel and the distribution position of the current abrasive grit i on the surface of the wheel. Thus, rotatory radius R_{si} of each active abrasive grit i around the machine tool spindle center O is calculated with the determination of the wheel substrate radius, the eccentric installation error of the abrasive wheel, and the initial position of the grit.

2.3 Theoretical Model of Cutting Depth of Active Grit in Peripheral-Sectional Plane

As shown in Fig. 1c, the machined scratch grooves are regularly removed with a certain material removal rate in one normal direction. The newly formed grooves are generated by the interaction between the continuously working abrasive grits distributed along the axial direction of the workpiece in the grinding contact zone with different grinding radii combined with the wheel substrate radius, protrusion height of the abrasive grit, and the eccentrical error of the wheel. Some grits cannot effectively remove the material because their protrusion heights are lower than the valley-position of the previously generated surface. This situation also occurs in the peripheral-sectional plane shown in Fig. 1d. The corresponding surface roughness is measured along the axial direction. Selecting an active grit at an instant of time t shown in Fig. 1b and one temporary reference coordinate system $X'' - Y''$ at the cutting point p in normal and peripheral directions is established. The enlarged trajectory paths of the adjacent abrasive grits are illustrated in Fig. 1d. The continuously incremental cutting depth of active abrasive grit in the peripheral- sectional plane is calculated as:

$$h_{r,i}(\varphi_i) = -h_g(\varphi_i) - \Delta h(\varphi_i) + h_w(\varphi_i), \tag{2}$$

where $h_g(\varphi_i)$ is the theoretical cutting depth of a single active grit and it is usually taken as the cutting depth in most of previous research; $\Delta h(\varphi_i)$ is the dynamic deviation from the normal cutting depth derived from the eccentrically rotational behavior of the abrasive wheel, which is deduced in detail in reference [18,19]; $h_w(\varphi_i)$ the local amplitude of peak-point on the initial surface waviness of the workpiece, which is always neglected and will be substituted by the surface waviness amplitude newly generated in the prospective material removal process.

In Equation (2), as shown in Fig. 1a and Fig. 1d, the theoretical cutting depth is calculated as [4,9]:

$$h_g(\varphi_i) = f_t \sin(\varphi_i), \quad 0 \le \varphi_i \le \Omega, \tag{3}$$

where $f_t = \lambda_s \cdot (v_w / v_s)$ is the feed rate per rotation of the abrasive wheel; v_w feeding speed of the workpiece; v_s is the peripheral speed of the abrasive wheel; and λ_s is the average distance between the adjacent active grits on the surface of the abrasive wheel, which is determined by the grinding wheel substrate diameter and the distribution and size of abrasive grits, and here assumed to be the same in both axial and peripheral directions and keeps constant under the same experimental conditions. $\varphi_i = \omega t$ is the rotatory position angle of the grit around the center of the machine tool spindle. The variable t is defined as total time from the grit cutting-in to cutting-out contact zone and can be discretized when calculating the rotatory position angle. The variable φ_i is very important for determining the working position of each active grit, the corresponding peak-points and valley-points of new-formed surface waviness, and surface roughness as well. The limit value of Ω is the radial cutting-in angle of the grit [6], as shown in Fig. 1a, which is used to determine the effective interaction area. The angle ϕ is defined as the effective included angle between the peripheral direction of the grit trajectory and the normal direction while current abrasive grits scratch through the contact zone, and is calculated as:

$$\cos\phi = \frac{a_p}{l_p},$$

where l_p is the length of a single scratch groove, shown in Fig. 1b (top-left view) and approximately calculated as [13]: $l_p = \sqrt{a_p \cdot d_s}$,

then: $\Omega \approx 2\arccos\sqrt{\dfrac{a_p}{d_s}}$,

when the rotatory position angle of the grit $\varphi_i > \Omega$, it indicates that the working grit tends to leave the grit-workpiece interaction zone, and the cutting depth turns to zero.

The dynamic deviation of the normal cutting depth $\Delta h(\varphi_i)$ in Eq. (2) is calculated as:

$$\Delta h(\varphi_i) = R_w(t) - R_w(t - T), \tag{4}$$

where $R_w(t)$ represents the actual rotation radius of active grit and is calculated as:

$$R_w(t) = \sqrt{R_{si}^2 + \delta_e^2 - 2R_{si}\delta_e \cos(\theta_s)}, \tag{5}$$

where $\theta_s = \angle PO'O = |\varphi_e - \varphi_i|$ is the rotation included angle from the machine tool spindle center to the eccentrically rotational center of the abrasive wheel; $\varphi_e = \varphi_{e0} + \theta$ is the position angle of the abrasive wheel center relative to the machine tool spindle center; $\theta = -\omega t$ is the dynamically rotatory angle of the wheel center at instant time t. Substituting the variables into Eq. (5), $R_w(t)$ becomes:

$$R_w(t) = \sqrt{R_{si}^2 + \delta_e^2 - 2R_{si}\delta_e \cos(|\varphi_{e0} - 2\omega t|)}. \tag{6}$$

2.4 Theoretical Model of Microcosmic Surface Topography with Discrete Method

The trajectory paths of consecutively active abrasive grits in a peripheral direction are illustrated in Fig. 1d. Accordingly, when the periodical time t that is taken for an active single abrasive grit from the cutting- in contact zone to cutting-out, the zone is discretized by k times with time interval T, i.e., $T = t/k$, and the material is removed by each working grit at a different cutting position with its own eccentrically rotating radius. Then, the incremental cutting depth that is expressed as the third variable in Eq. (2) by removing the previously generated wavy surface or initial surface of the workpiece, is approximately characterized with the discrete method as:

$$h_w(\varphi_i) = y_a \sin(\omega t / k + \Phi_i). \tag{7}$$

The characteristic value of surface waviness remains varied as time passes, and the grinding trajectory paths of eccentrically rotating grits change dynamically. In Equation (7), k represents the sampling times within the length of the workpiece surface. The symbol m is the number of active abrasive grits simultaneously working in the contact zone in a peripheral direction. The complete surface waviness generated in the grinding process is restructured and connected with multiple segmented surface waves separately generated by various abrasive grits along their grinding trajectory paths. In order to improve solution precision, the surface waviness could be evenly segmented into at least 4 sections of regular sinusoidal fluctuation, i.e. $k=4Nm$ ($N=1,2,\ldots$), which implies that more discretized peak- or valley-points of the surface are solved. To simplify the calculation, here variable k is set to be equal to $4m$ ($N=1$), which implies that the discretized surface waviness of the workpiece is generated and restructured with only one individual sinusoidal fluctuation formed by abrasive grits m during the cutting-in and cutting-out process. Although the assumption may cause a little error variation, it will not have a significant impact on the acquisition of peak- points and valley-points of whole surface machined. ϕ_i is the phase difference between the motion trajectory of adjacent abrasive grits in a peripheral direction and their varying eccentrically rotational radius, and is approximately calculated by the respective position phase in a sinusoidal trajectory path.

The amplitude variable of y_a in Eq. (7) is defined as the average longitudinal height between peak- and valley-points in k sampling times along a peripheral direction and described as:

$$y_a = \frac{1}{k_n}\sum_{x=1}^{k_n} R_{a,wx}, \tag{8}$$

where k_n is the sampling times in each sampling zone for measuring the whole surface roughness. By means of discretization in unit distance interval Δx, the variable $R_{a,wx}$ represents the average longitudinal height between peak- and valley-points in local surface topography. Thus, Eq. (7) is used to restructure the initial surface topography based on surface roughness measured prior to grinding. By substituting the expression of the initial surface to the corresponding trajectory path of eccentrically rotating abrasive grits, the incremental cutting depth is obtained, and newly generated surface topographies are quantitatively characterized by peak- and valley-points in the scratch grooves. The influence of the characteristics of the initial surface waviness of the workpiece on instantaneous cutting depth is discussed in the subsequent experiment section.

Substituting above Eqs. (3), (4) [18,19] and (7) into Eq. (2) after discretization with DM, the complete expression of the microcosmic surface topography is further depicted as:

$$h_r(\varphi_i) = -f_t \sin(\omega t) - \Delta h(\omega t) + y_a \sin(\omega t / k + \Phi_i), \tag{9}$$

$$h_r(\varphi_i) = -f_t \sin(\omega t) - \frac{1}{k}\sum_{i=1}^{k}\Delta h(\omega t)\cos(i\omega T) + \frac{1}{k}\sum_{i=1}^{k} y_a \sin(i\omega T + \Phi). \tag{10}$$

The physical meanings of Eqs. (9) and (10) are that under excitation frequency of the eccentrically rotational behavior of active grits in contact zone, the material is removed with various grinding radii and cutting depth $h_r(\varphi_i)$, then the periodical surface waviness is generated by connecting discretized k segmented wavy surfaces. The fluctuating frequency of the discretized surface waviness is approximately constant, while the amplitudes of the waves are undulant due to various rotatory trajectory of each working grit.

The model of an instantaneous cutting depth of a single grit in Eqs. (9) or (10) consists of two parts. The first part is related to the feed cutting depth per rotation based on motion trajectory combined with the feed motion of the workpiece and the rotatory motion of the abrasive wheel. The second part is related to the dynamic cutting depth derived from the eccentrically rotational behavior of the abrasive wheel as well as the incremental deviation between previous and newly generated surface waviness respectively. The condition applied to the improved model of cutting depth is closer to the actual machining situation in higher prediction precision. As the value of the feed cutting depth per rotation is significantly larger than that of the dynamic cutting depths, the value of the instantaneous cutting depth $h_r(\varphi_i)$ reaches the maximum at the moment abrasive grits cut into the critical boundary of the grinding contact zone (i.e., $\varphi_i = \Omega$) and decreases gradually as the process lasts. With the superposition of the instantaneous impact of abrasive grits cutting into the eccentrically rotating abrasive wheel–machine tool spindle system, the total amplitude of the vibration and motion trajectory of active abrasive grits will correspondingly increase. With the movement of the eccentrically rotating abrasive wheel, while the cutting point p of current active grit and the rotatory center O of abrasive wheel coincide with the rotatory center O' of the machine tool spindle in a line, that is, $\varphi_{e0}=2\omega t$ or $t=\varphi_{e0}/(2\omega)$, the dynamic cutting depth derived from the eccentrically rotational behavior of the abrasive wheel decreases to minimum, and the forced vibration excited from the abrasive wheel-machine tool spindle will keep relatively stable in a lower amplitude range due to the cutting point p with the eccentricity value staying far away from the critical boundary of contact zone.

2.5 Theoretical Model of Microcosmic Surface Roughness

The total normal cutting depth of continuously active grits simultaneously removing material in the contact zone can be calculated by Eq. (11), and the surface roughness of the machined workpiece is expressed in Eq. (12) as:

$$h_r = \sum_{i=1}^{m}\left|h_r(\varphi_i)\right|, \tag{11}$$

$$R_a = \frac{1}{k}\sum_{i=1}^{k}\left|h_r(\varphi_i)\right|. \tag{12}$$

To verify the validity and prediction precision of the surface roughness model in Eq. (12), two engineering empirical formulas from references [20,21] are introduced separately as:

$$R_a = 0.256\max\left(2\left|h_r(\varphi_i)\right|\right), \tag{13}$$

$$R_a = 1.36\lambda_{sl}^{6/5}\left(\frac{f_t}{B_s}\right)^{2/5}\left(\frac{v_w}{v_s}\right)^{2/5}\left(\frac{1}{2R_{si}}\right)^{1/5}. \tag{14}$$

In these two empirical formulas, most variables have been introduced in previous sections except that B_s is the width in axial direction or thickness of the abrasive wheel. The prediction precisions of three formulas are compared and the application limitations of them are analyzed in subsequent sections.

2.6 Influence of Morphology Characteristics of Abrasive Grits Geometries on Microcosmic Surface Generation

As shown in Fig. 1c, the instantaneous values of peak-points ($v_1 - v_n$) and valley-points ($w_1 - w_n$) are obtained by calculating the intersection of the previous surface waviness and currently moving trajectory of abrasive grits with various geometries morphology. In actual machining process, the main morphology of working grits is usually assumed to be conical, cuboid, spherical and their combinations [22] according to the variable of relative area ratio between top area and bottom area, as listed in Table 1. There is a small difference in machining performance if the proportion of three types of grit geometries changes. In this study, the corresponding relationship between the cutting depth in a peripheral direction and the size of three types of working grits geometries is investigated and illustrated in Fig. 2.

Table 1. Main morphology of working abrasive grits

Morphology categorization			Characteristics formulae	Projection disambiguatation
Group	Sub-type	Geometry	Criterion	Features
		Sphere	$S_1/S_2 \geq 0.8$	None
		Ellipsoid	$S_1/S_2 < 0.8$	
		Triangular pyramid	$S_1/S_2 \leq 0.1$	Three edges and one highlight peak
		Rectangular pyramid		Four edges and one highlight peak
		Pentahedron		Five edges and one highlight peak
		Rhombo-hedron		Six edges and one highlight peak
		Cone	$S_1/S_2 \leq 0.1$	Round bottom-surface and one peak
		Truncated cone	$0.1< S_1/S_2<0.8$	Round bottom-surface and one top-surface
		Cylinder	$S_1/S_2 \geq 0.8$	Round bottom-surface and one top-surface
		Triangular prism	$S_1/S_2 \geq 0.8$	Three edges and one truncated top-surface
		Quadrangular prism		Four edges and one truncated top-surface
		Pentahedral prism		Five edges and one truncated top-surface
		Rhombohedral prism		Six edges and one truncated top-surface

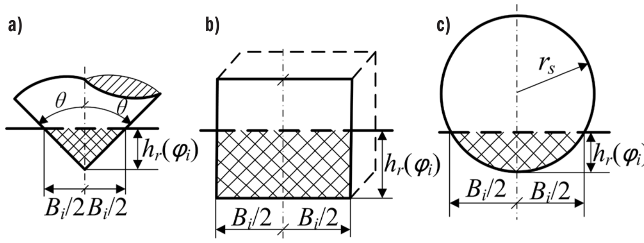

Fig. 2. The corresponding relationship between cutting depth in peripheral direction and geometric sizes of abrasive grits; a) conical; b) cuboid; and c) spherical

According to the material removal mechanism in Fig. 1b, the morphology characteristics of abrasive grits and maximum cross-section areas in contact with surface waviness are shown in Fig. 2. Neglecting the influence of plastic flow and pile-up of material, the maximum surface areas of the longitudinal cross-sections (such as the shadow zone in Fig. 2) of the material removed by single grit i with three geometry types can be calculated respectively as:

a) For conical abrasive grits: $B_1 = 2\,h_r(\varphi_i)\tan(\theta)$, then the section area of one groove by single abrasive grit is calculated as:

$$S_1 = \frac{1}{2} B_i h_r(\varphi_i) = h_r^2(\varphi_i) \cdot \tan\theta.$$

b) For cuboid abrasive grits, the ratio of length to width of a single grit is simplified to be 3:2, then $B_2 = 4/3\,h_r(\varphi_i)$, and the section area of one groove by single grit is calculated as:

$$S_2 = B_i \cdot h_r(\varphi_i) = \frac{4}{3} h_r^2(\varphi_i).$$

c) For spherical abrasive grits: $B_3 = 2\sqrt{(2r_s - h_r(\varphi_i))h_r(\varphi_i)}$, then the section area of one groove by single grit is calculated as:

$$S_3 = r_s^2 \arcsin\left(\sqrt{2\frac{h_r}{r_s} - \left(\frac{h_r}{r_s}\right)^2}\right).$$

By accumulating the surface area of continuously working abrasive grits with different geometries proportioned at the same interval, it can be calculated as:

$$S_n = \sum_{j=1}^{3} (S_j\, W_{nj}), \tag{15}$$

where W_{nj} is the proportion of numbers of active grits with one type of geometry compared to the total number of effective abrasive grits. It is assumed that the proportion is approximately equal in different grit distribution zones, then $W_{n1}+W_{n2}+W_{n3}=1$. By scanning the cross-section of grit geometries along the trajectory path of material removed, the coordinate values of interaction points between the normal-sectional plane of the workpiece and the cross-section of abrasive grit geometries are obtained. The maximum and minimum values of interaction points are characterized as peak-points and valley-points of surface roughness and used to predict machining accuracy.

The incremental cutting depth of effective working grits is comprehensively considered in Eq. (15). Furthermore, if the geometric sizes of the overlapping grooves are larger than the distance λ_s that is related to the instantaneous cutting depth of abrasive grit, then during some interval T, the correspondingly incremental volume V_w of instantaneously-removed material along the motion trajectory of abrasive grits cutting-in and cutting-out of the material can be calculated as:

$$V_w = S_n l_p = S_n \sqrt{a_p d_s}, \quad \text{if} \quad \lambda_s \geq B_i, \tag{16}$$

$$V_w = (S_n - \lambda_s h_r(\varphi_i)) l_p = (S_n - \lambda_s h_r(\varphi_i))\sqrt{a_p d_s}, \quad \text{if} \quad \lambda_s < B_i. \tag{17}$$

Equation (16) is commonly taken as the theoretical formula to calculate average material removal volume in most research [1,13]. In both Eqs. (16) and (17), the judging condition is to determine if the overlapping situation of the scratch grooves occurs, as illustrated in Fig. 1c. When the value of the width of the effective section of a single abrasive grit is larger than the distribution distance of adjacent grits, a certain amount of the workpiece material is incrementally removed as the consecutive scratch grooves overlap, instead of substituting the whole cross-sectional area of single grit in order to calculate the material removal volume. Thus, the calculation value with Eq. (17) is lower than the one with Eq. (16). With the increase of grinding stability and the distribution uniformity of an instantaneous cutting depth, the prediction precision increases, which is verified on the basis of comparison analysis in the following experimental section.

2.7 Experimental Conditions and Data Analysis Methods

Five groups of rough grinding and precision grinding experiments were carried out on the same precision grinder Jones and Shipman 540 (Jones and Shipman, UK), respectively. The experimental principle and measuring platform are illustrated in Fig. 3 and the main grinding parameters are listed in Table 2.

Table 2. Experimental conditions of surface grinding

Preset cutting depth [μm]	5, 15
Spindle speed [r/min]	2880
Workpiece feed speed [mm/s]	150
Eccentricity value of abrasive wheel [μm]	1, 2, 3
Initial installation position angle of abrasive wheel center [º]	30

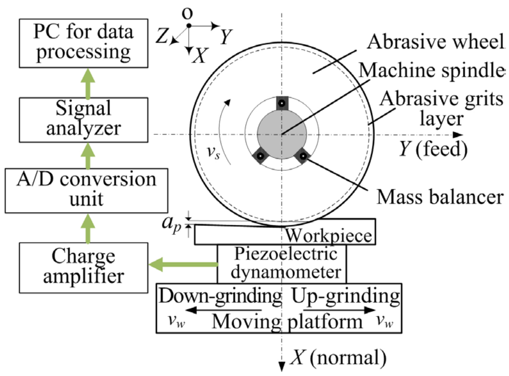

Fig. 3. Experimental principle and measurement platform of surface grinding process

Prior to every grinding experiment, the eccentricity value of the grinding wheel is calibrated and corrected with a static/dynamic balancing instrument NHY-2000-810A (Sigma, Japan) in order to decrease the disturbance errors in the eccentricity value fluctuation. This is achieved by adjusting the installation position of the mass balancer shown in Fig. 3. This ensures that the eccentricity value of the grinding wheel is effectively controlled within 1 µm, 2 µm and 3 µm according to the experimental needs. During experiments with micro-grinding or precision grinding with low material removal rate, the eccentrically rotational behavior of the abrasive wheel is examined by the in-situ dynamic balancer instrument CB-2001RGB (Sigma, Japan) installed on the motorized spindle. The process monitors the deterioration of the eccentrical vibration of the abrasive wheel with consideration of the changes in wheel wear in order to insure the eccentricity value fluctuates in the error range of ±5 % of preset one during grinding. The characteristic value of surface topography and surface roughness are measured, and the data analysis is implemented.

A monolayer resin-bonded diamond abrasive wheel with electroplated grits is applied to conduct grinding experiments. The abrasive wheel specification takes values of substrate diameter ϕ 162 mm, width 20 mm and abrasive particle size number 200/230# by ANSI-B74.16 [23]. The average size of abrasive grits is 750 µm and adjacent grits spacing is 500 µm. Considering better performance of material removal and chip formation that is beneficial for measuring peak- and valley-points of machined surface topography, the medium carbon-steel EN8 (surface size: length 20 mm × width 10 mm) is selected as sample material. The workpiece is fixed on the worktable with mode of single-pass down-grinding without lubricant, which implies that the dynamic wear of the grind wheel between two adjacent experiments is almost negligible. The material properties, machinability and composition of the sample workpiece are listed in Tables 3 and 4, respectively. The piezoelectric acceleration sensor Kistler 8764B and dynamometer Kistler 9257BA (Kistler Group, Switzerland) are assembled to measure the vibration acceleration signal and grinding force signal of the workpiece in the feed direction (motion direction of the worktable) and the normal direction (perpendicular to motion direction of the worktable), and the sampling frequency of two sensors are set to 50 kHz. The collected signals, after conversion by the charge amplifier and the A/D unit PMD-1608FS (MCC, US) where phase characteristics are also calibrated prior to every grinding experiment and are input to the signal analyzer CSI3005III (Emerson, US) and the computer equipped with graphic data analysis software LABVIEW (Ni Solutions, Sweden) for vibration signal analysis. Within the sampling length range of 5 mm on the machined surface, five different zones are randomly selected to measure surface topography. The mean values of the surface topography characteristics (including peak- and valley-amplitude of surface waviness, length and width of contact zone) are measured and the corresponding data analyses are conducted after each group of grinding experiments to effectively decrease initial noise errors of surface roughness measurement on the surface roughness profiler Talysurf6 (Taylor Hobson, UK).

Table 3. Material properties and machinability of workpiece

Heat treatment mode	normalizing treatment	Yield strength [MPa]	≥360
Hardness [HB]	170-210	Tensile strength [MPa]	600-750
Elastic modulus [GPa]	210	Elongation [%]	≥15

Table 4. Composition of workpiece material

C [%]	Si [%]	Mn [%]	P [%]	S [%]
0.35-0.45	0.05-0.35	0.6-1	≥0.06	≥0.06

3 RESULTS AND DISCUSSION

3.1 Measurement and Restructure of Initial Surface Topography of the Workpiece

The quantitative influence of characteristics distribution of the initial surface topography is studied by rough grinding experiments with conditions of δ_e=1 µm, f_t=0.3 µm, a_p=15 µm. The initial surface topography enlarged 20 times is shown in Fig. 4a. Surface roughness after grinding from two randomly selected sampling zones (1) and (2) in Fig. 4b, whose values are 0.49 µm and 0.55 µm are measured along a perpendicular direction to the grinding direction. The reconstruction of the machined surface waviness in X−Z sectional plane is conducted by Eq. (10) with values of peak-points and valley-points extracted from the sampling zones. The corresponding 3D machined surface topographies are obtained, as shown in Fig. 4c and d.

According to the analysis of the grinding kinematic and microcosmic surface generation in Section 2, surface topography is affected by the main process parameters, grit morphology, position distribution and protrusion height distribution regularity of working grits with different particle sizes. It is shown that the 3D surface topography in Fig. 4 presents a grinding situation of continuously active grits scratching through the contact zone with unequal protrusion heights (i.e. cutting edges with unequal height) of the adjacent distributing abrasive grits and with incremental cutting depth. The staggered and overlapped scratch grooves were left with characteristic values of peak-points and valley-points. The longitudinal distance between the maximum peak-point and the deepest valley-point of the scratches is about 0.6 µm almost double that of f_t by multiple abrasive grits scratching through the same position. By further extraction and calculation using Eq. (11), the average total cutting depth of each grit is about 13.87 µm with an error of 1.13 µm compared with a_p=15 µm at a proportion of 7.5 %. The error of average cutting depth is explained that the initial surface waviness and the eccentricity value of the abrasive wheel of 1 µm are introduced in Eq. (9).

3.2 Surface Topography of Workpiece in Peripheral Section under Condition of Eccentrical Rotation Excitation of Abrasive Wheel

Two groups of precision grinding experiments are designated with conditions of f_t=0.1 µm, a_p=5 µm, and conducted to verify the validity and prediction precision of the discretized theoretical models of microcosmic surface topography by comparison with experimental data and simulation outputs, where the length of the sampling zone is 0.5 mm.

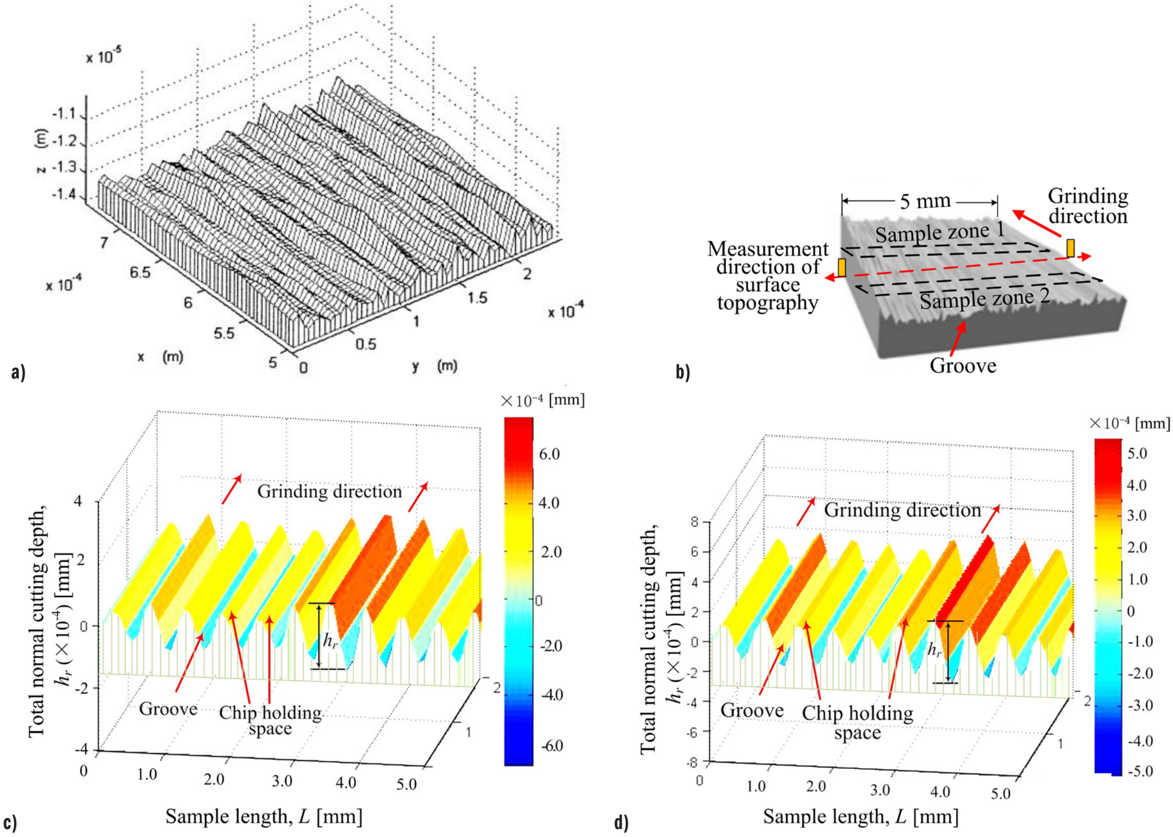

Fig. 4. 3D surface topography; a) initial surface topography; b) sampling zones for measuring surface topography; c) simulated surface topography in sampling zone 1; and d) simulated surface topography in sampling zone 2

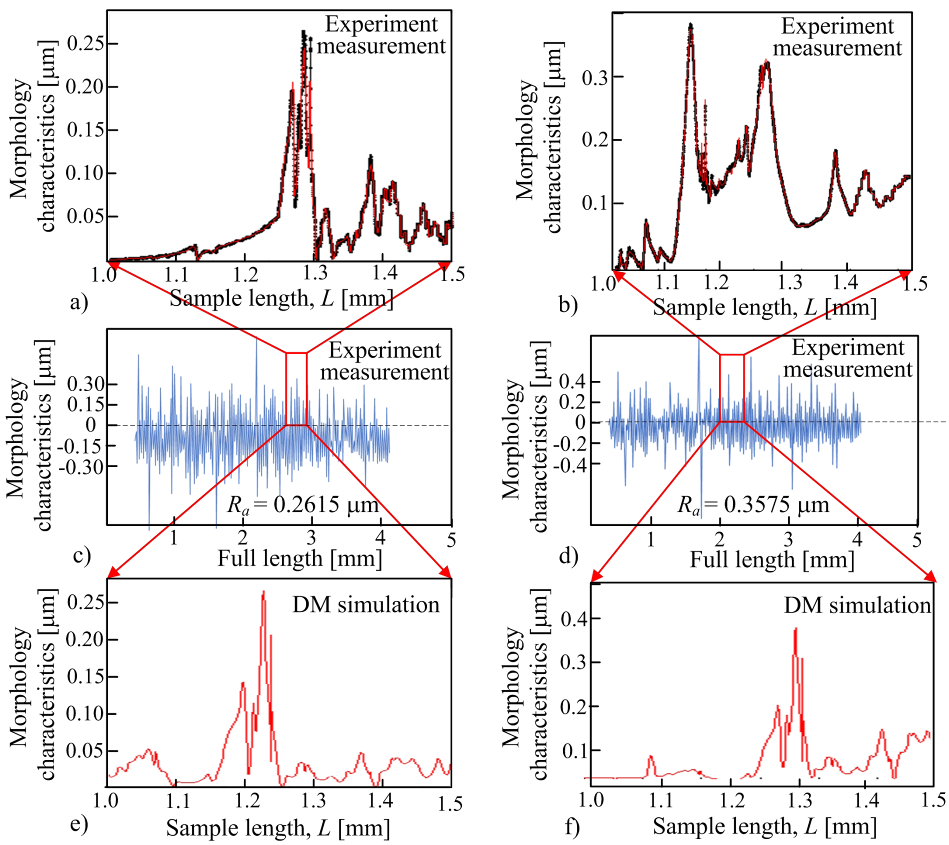

Fig. 5. Morphology characteristics of workpiece when δ_e are set to 1 μm and 2 μm; a) and b) enlarged surface topography by experiments; c) and d) actual surface topography by experiments; e) and f) enlarged surface topography by DM simulation

The first group of experiments is conducted with an eccentricity rotational value of the abrasive wheel of 1 µm. Surface roughness of the machined workpiece is measured and the corresponding characteristic value of surface topography, including peak-points and valley-points are extracted and used to restructure microcosmic surface topography with full discretization Eq. (10). The characteristics of the initial surface topography value is considered prior to precision grinding. As illustrated in Figs. 5c, a and e, respectively, surface waviness is enlarged to observe the local characteristics obtained from experiments, using a full discretization simulation. The experiments that specify eccentricity rotational values of the abrasive wheel at 2 µm by adjusting the mass balancer position and using a_p = 5 µm, are conducted by continuously utilizing the workpiece machined under the condition of an eccentricity value of 1 µm. The characteristics of surface topography are measured and extracted with the same data-processing principle above, and the corresponding results are shown in Figs. 5d, b and f.

In Fig. 5c, the surface roughness of 0.2615 µm with δ_e of 1 µm is better than that of 0.3575 µm with de of 2 µm as shown in Fig. 5d, which implies that the former is smoother than the latter. Surface roughness of the latter deteriorates approximately by 37 %. By comparing the local characteristics of the surface waviness in details shown in Figs. 5a and b from experiments with the discretization simulation outputs shown in Figs. 5e and f, it is shown that the common tendency of the two results is, at some discrete moment, the total amount of instantaneous cutting depth of continuously effective abrasive grits in the peripheral plane improves up to the maximum as the static or theoretical cutting depth, the absolute value of first variable in Eqs. (9) or (10), keeps a higher proportion. Meanwhile, a stronger dynamic impact exists when the error rate of abrasive grits cutting into the material increases with an increase of the eccentrically rotational excitation. As the process becomes gradually stable, the instantaneous cutting depth distinctly decreases and keeps a small fluctuation with a cutting depth per rotation of 0.1 µm. With the increase of δ_e from 1 µm to 2 µm, the effective grinding radius of variable R_{si} of a single grit in the contact zone increases according to Eq. (1) and the depiction in Fig. 1. Accordingly, the instantaneous cutting depth in a local region distinctly increases to almost 2 times, and surface roughness of the latter is larger by 1.37 times than the former. The tendency implies that the grinding stability deteriorates, and serious vibration occurs. In comparison of the characteristics of peak-points and valley-points from the experiments and restructure simulations, both the fluctuation tendency of surface waviness coincide very well. The prediction error was about 50 %. But when δ_e is 1 µm, the error decreases to within 20 % when δ_e is 2 µm. This indicates that on a condition of stable grinding, the total predicted amount of cutting depth is lower as the characteristics of the initial surface topography are considered in the third variable in Eq. (9) when calculating total instantaneous cutting depth. The particle size, distance distribution and grinding preference of abrasive grits have a small influence on the material removal process during micro-grinding as well. Unlike the situation in which eccentrical vibration increases, the influential proportion of the incremental cutting depth in the second variable in Eq. (9) derives from eccentric rotational behavior increases, which results in the descending influential proportion of the morphology characteristics of abrasive grits. Such considerations result in predictions closer to actual grinding situations.

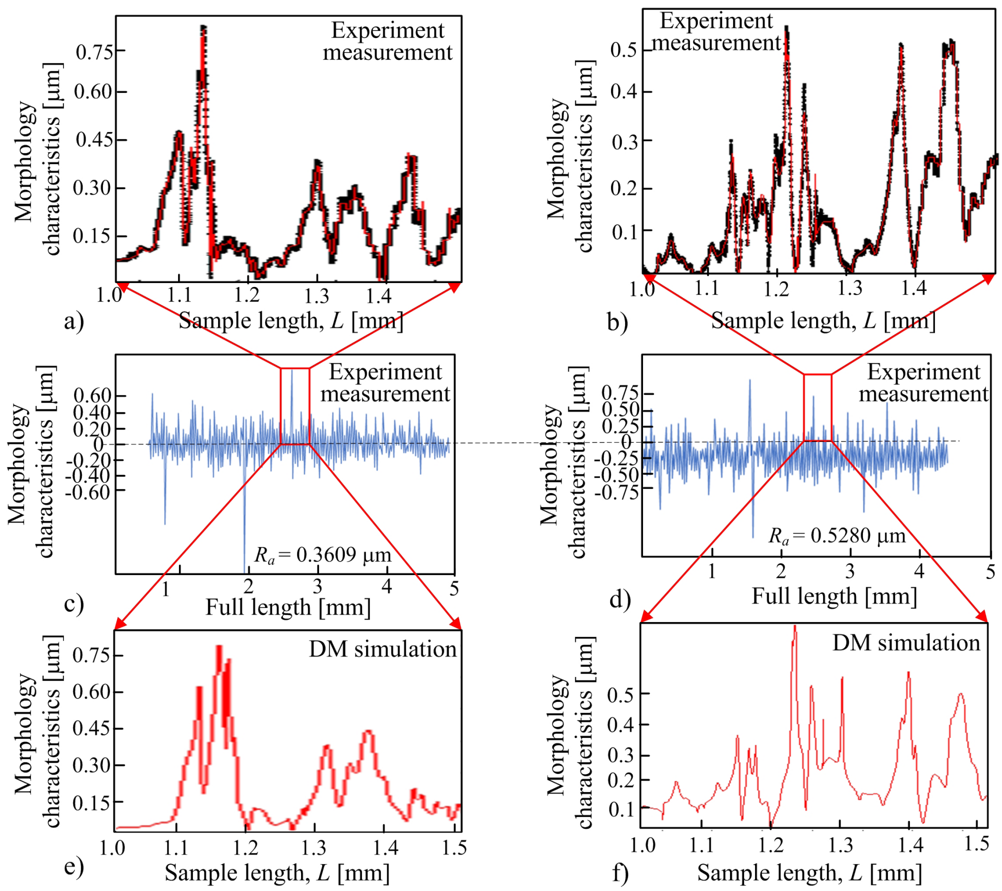

Fig. 6. Morphology characteristics of workpiece when δ_e are set to 2 µm and 3 µm; a) and b) enlarged surface topography by experiments; c) and d) actual surface topography by experiments; e) and f) enlarged surface topography by DM simulation

The second group of experiments are conducted by referring to the same technique and data analysis when δ_e turn to 2 µm and 3 µm (the upper limit value of stable grinding in most research). Separately, the responding characteristic values of surface waviness and surface roughness are measured and restructured. Surface waviness is enlarged to observe local characteristics as obtained from experiments and full discretization simulations are illustrated in Fig. 6a to Fig. 6f respectively.

In Fig. 6c, the surface roughness of 0.3609 µm with δ_e of 2 µm is better than 0.5280 µm with δ_e of 3 µm shown in Fig. 6d, which implies that the former is distinctly better than the latter in smoothness of surface waviness, where the surface roughness of the latter deteriorates approximately up to 47 %. Compared with the local characteristics of surface waviness shown in Figs. 6a and b from experiments and the discretization simulation outputs in Figs. 6e and f, the results imply the tendency is similar to the situation of the aforementioned paragraph. In other words, with the increase of δ_e from 1 µm to 2 µm, the local characteristics values increase greatly, and the tendency of experimental data and simulation outputs coincide very well etc. Though δ_e only ranges from 2 µm to 3 µm, the instantaneous cutting depth in the local region distinctly increases to approximately 46 %. However, the prediction error decreases to within 10 % when the eccentricity value is 3 µm. It indicates that with the development of stronger eccentrical vibration, the influential proportion of the incremental cutting depth derived from the eccentric rotational behavior increases significantly and even closely approximates to the static or theoretical one, which results in prediction outputs closer to the actual grinding situation where the error is approximately 10 %.

3.3 The Prediction Precision Analysis of the Improved Theoretical Models of Surface Roughness and Incremental Material Removal Volume

Using experimental protocols with δ_e ranging from 1 µm to 3 µm, and substituting the process parameters in Table 2 and the characteristics values (including peak-points and valley- points of surface waviness), into the theoretical models of surface roughness in Eq. (12) (with DM) and empirical Eqs. (13) and (14) respectively, the corresponding prediction results of surface roughness in conditions of changed speed ratio between the feed speed of the workpiece and the peripheral speed of the abrasive wheel from 0.006 to 0.012 are illustrated in Fig. 7.

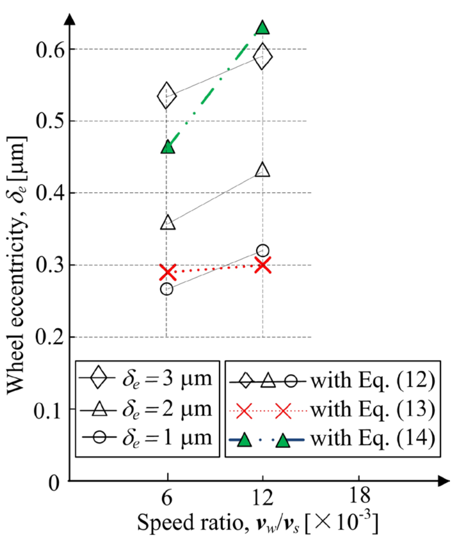

Fig. 7. Surface roughness obtained from experimental data, DM model and two fitting formulas

In Figure 7, the prediction values of surface roughness in accordance with 'dynamic deteriorated' δ_e from 1 µm, 2 µm to 3 µm in Eq. (12) are 0.26 µm, 0.36 µm, 0.53 µm respectively when the lower speed ratio is adopted, i.e. at a low feed speed of the workpiece or a high peripheral speed of the abrasive wheel. The value of surface roughness obtained in simplified Eq. (13) is 0.27 µm, which is similar to the stable situation (δ_e = 1 µm), and the prediction error is almost 4 %. The value of surface roughness obtained in complicated Eq. (14) is 0.48 µm similar to the result of a relatively unstable grinding state (δ_e = 3 µm), where the prediction error is almost 9 %. The tendency indicates that the physical considerations in Eq. (13) are mainly based on the material removal process with a crucial index of instantaneous cutting depth to predict machining accuracy in accordance with the actual grinding process. Meanwhile, Eq. (14) coincides with the situation considering various nonlinear influential factors of the process parameters. The prediction errors are 25 % and 33 % respectively when comparing the values in Eqs. (13) and (14) using the prediction value in Eq. (12) with δ_e of 2 µm.
Furthermore, the prediction values of surface roughness with δ_e of 1 µm, 2 µm, 3 µm in Eq. (12) are 0.32 µm, 0.43 µm, 0.58 µm respectively when the higher speed ratio is adopted. The value of surface roughness obtained in simplified Eq. (13) and complicated Eq. (14) are 0.30 µm and 0.63 µm, respectively. Both results are also similar to those in stable and unstable situations. The result demonstrates that Eqs. (13) and (14) are suitable to approximately predict the machined accuracy level compared with the outputs in Eq. (12). The analysis further indicates that Eq. (13) is more suitable to be utilized to predict surface roughness in a stable grinding process, especially in micro-grinding, i.e. the instantaneous cutting depth stays even. The prediction accuracy improves when the mean value of maximum cutting depth in several sampling zones is adopted, i.e. the formula is simplified and improved in the following formula: $R_a = 0.256\,\overline{\max(2|h_r(\varphi_i)|)}$. Equation (14) is more suitable to be utilized to predict surface roughness in various grinding process parameters, especially in rough grinding with a larger cutting depth.

To further improve the statistical reliability of the kinematic model for predicting surface roughness, the detailed peak-points (Peak-P) and valley-points (Val-P) are extracted from the experimental measurement (R_a-Exp) and prediction outputs (R_a-DM) based on Figs. 5 and 6, and depicted in Table 5 with the increase of δ_e. Here the sampling length of 0.5 mm is divided into 10 zones to measure the surface topography every 0.05 mm. In Table 5, it is shown that with the increase of δ_e, the maximum of Peak-P or Val-P (absolute value) from experiments are almost close to prediction outputs with the DM model. Meanwhile, the larger amplitude difference highlighted between Peak-P and Val-P occurs both in R_a-Exp and R_a-DM and increases significantly, which demonstrates that the instantaneous cutting depth of active grits is becoming deeper due to the deteriorated vibration excitation derived from the wheel rotating behavior with a larger eccentricity value.

According to the experiment protocol in varying δ_e from 1 µm to 3 µm and using the lower speed ratio, substituting the instantaneous cutting depth and the size of cuboid geometries of abrasive grits whose area is maximum in three types of geometries into the prediction model of total material removal volume per unit area in Eq. (16), (whose area variable is adopted with whole section area of working abrasive grits), and using the improved Eq. (17), (whose area variable is the incremental area considering overlapping situation of scratch grooves), the prediction results for average material removal volume with both Eqs. (16) and (17) are illustrated in Fig. 8. It is noted that the number of effective abrasive grits is the one working in some peripheral section along the wheel surface.

Table 5. Peak-points and valley-points of machined surface topography by experiments and DM model

Sampling zone	$\delta_e = 1\ \mu m$				$\delta_e = 2\ \mu m$				$\delta_e = 3\ \mu m$			
	R_a-Exp		R_a-DM		R_a-Exp		R_a-DM		R_a-Exp		R_a-DM	
	Val-P	Peak-P	Val-P	Peak-P	Val-P	Peak-P	Val-P	Peak-P	Val-P	Peak-P	Val-P	Peak-P
1.00-1.05	-0.020	0.007	-0.026	0.04	-0.02	0.05	-0.20	0.005	-0.15	0.10	-0.20	0.12
1.05-1.10	-0.025	0.009	-0.028	0.05	-0.25	0.08	-0.25	0.10	-0.35	0.05	-0.25	0.20
1.10-1.15	-0.026	0.02	-0.02	0.10	-0.10	0.38	-0.27	0.10	-0.30	0.30	-0.27	0.20
1.15-1.20	-0.18	0.04	-0.15	0.15	-0.25	0.26	-0.27	0.15	-0.23	0.25	-0.37	0.15
1.20-1.25	-0.12	0.20	-0.01	0.27	-0.20	0.20	-0.22	0.27	-0.25	0.55	-0.22	0.82
1.25-1.30	-0.08	0.27	-0.22	0.04	-0.15	0.32	-0.10	0.38	-0.25	0.40	-0.30	0.53
1.30-1.35	-0.19	0.05	-0.26	0.02	-0.27	0.10	-0.18	0.30	-0.18	0.36	-0.18	0.50
1.35-1.40	-0.20	0.06	-0.26	0.03	-0.20	0.20	-0.25	0.10	-0.15	0.52	-0.45	0.15
1.40-1.45	-0.17	0.12	-0.25	0.05	-0.02	0.15	-0.20	0.15	-0.02	0.54	-0.15	0.50
1.45-1.50	-0.25	0.07	-0.22	0.05	-0.25	0.14	-0.23	0.17	-0.10	0.54	-0.38	0.12

Meanwhile, the corresponding surface roughness and specific grinding forces within the workpiece length of 20 mm in normal and feed directions in conditions of the same process parameters with speed ratio 0.006 and various eccentricity values measured by experiments are illustrated in Fig. 9.

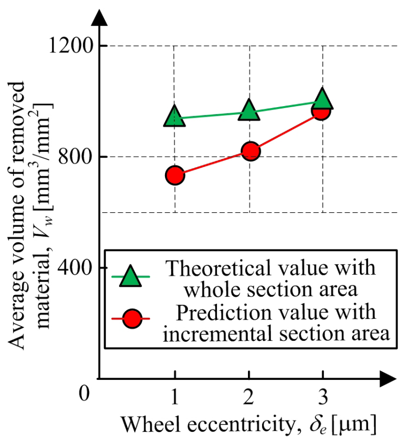

Fig. 8. Average volume of material removed by effective abrasive grits in contact zone

As shown in Fig. 8, it is assumed that the proportion of conical, cuboid, and spherical are 20 %, 60 %, and 20 %, respectively. In a stable condition of the same δ_e of 1 µm, as the whole section area of any type of grit geometry is obviously larger than the incremental section area of the continuously active grit removing material, the theoretical value of average material removal volume of 900 mm^3 obtained with Eq. (16) is distinctly larger than that of 720 mm^3 with the incremental Eq. (17), in which the error is about 25 %. A similar tendency occurs in surface roughness and specific grinding forces when the average material removal volume varies with the Eqs. (16) and (17), as shown in Fig. 9. With the increase of eccentrical vibration excitation when δ_e is 3 µm, the overlapping situation decreases the accumulated material removal volume removed by each working grit, accompanying the trend of slowing down in grinding forces in Figs. 9b and c. The incremental material removal volume of 860 mm^3 with Eq. (17) is further close to the theoretical one of 946 mm^3 with Eq. (16), in which the error is approximately by 10 %. The regularity of varying material removal volume is similar with surface roughness when the eccentricity value varies. Comparing the theoretical value of material removal volume, the prediction precision improves 19 % and 14 % with Eq. (17) when δ_e are 1 µm and 2 µm, respectively. The result demonstrates that both the prediction models of incremental material removal volume and the model of surface roughness are

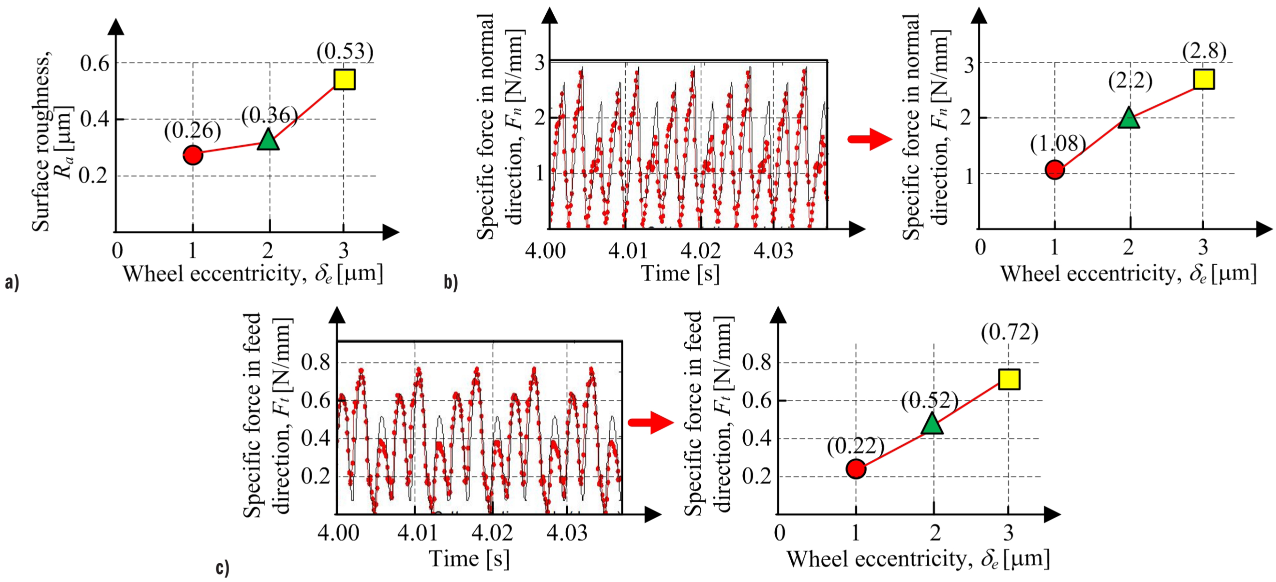

Fig. 9. Surface roughness and specific grinding forces with the increase of wheel eccentricity values; a) Surface roughness by experiments; b) Specific grinding force in normal direction by experiments and evolution trend; c) Specific grinding force in feed direction by experiments and evolution trend

more suitable for engineering application in the actual grinding process.

4 CONCLUSIONS

It is a key research issue to monitor grinding quality, control process stability, and acquire a high-quality machined surface in order to understand profoundly the influence of various linear and nonlinear factors on the material removal mechanisms in the generation of the final machined surface topography of the workpiece. In this paper, the comprehensive effects of nonlinear factors, such as the initial surface waviness of the workpiece, the eccentrically rotational behavior of the abrasive wheel and the morphology combination of abrasive grits on the instantaneous/dynamic cutting depth are depicted systematically, and the improved prediction model for microcosmic surface topography is presented by utilizing a discrete method and restructuring technique. By comparing grinding experiments, previous empirical engineering formulas, and 2D and 3D simulation results, the reliability of the prediction model of surface topography is verified. The models proposed in the paper are practical for predicting the microcosmic surface topography and its generation in higher accuracy in cases of rough grinding, precision grinding and even micro-grinding processes. The important conclusions of this study include:

1. In micro-grinding or precision grinding with a low removal rate, both the initial surface waviness and the eccentric rotational behavior of the abrasive wheel have a significant influence on grinding process stability and surface topography generation but are commonly neglected in most of previous research. By comparing experimental data and simulation outputs from theoretical models of surface topography including peak- and valley-points, and the surface roughness under varying conditions of eccentricity rotational values, the improved theoretical model of microcosmic surface topography can reliably calculate the characteristic value of peak and valley of surface topography under complex conditions in considering the influential factors above. With an increase in the eccentricity rotational values of the abrasive wheel, the prediction precision of microcosmic surface topography increases with an error of 10 %.
2. Compared to the theoretical model of surface topography in Eq. (12), in considering varying eccentricity rotational behaviors of the abrasive wheel, the prediction result based on the simplified model of surface topography with Eq. (13), which is an empirical engineering formula, is closer to stable process with an error of 4 % when the eccentricity rotational value is 1 µm, while the prediction result based on the complicated model of surface topography with Eq. (14), which is another empirical engineering formula, is closer to a relatively unstable process with an error of 9 % to 19 % when the eccentricity rotational value is 3 µm.
3. Compared to commonly used theoretical model of material removal rate, which takes a whole section area of abrasive grit geometry as a variable, under varying eccentricity rotational conditions, the improved model of material removal volume comprehensively considers both the overlapping status of scratch grooves formed by continuously working abrasive grits and the morphology combination of abrasive grits geometries. Thus, the improved model is suitable for predicting the actual grinding situation with higher accuracy. The prediction accuracy for material removal volume with the improved model in this paper improves almost 9 % by adopting the maximum of the eccentricity rotational value of 3 µm, and approximately 19 % and 14 % by adopting the eccentricity rotational values of 1µm and 2 µm respectively, relative to the results derived from the commonly used theoretical model.
4. The quantitative assessment of machining quality demonstrates that surface roughness generated in precision grinding increases significantly when a stable grinding process tends to instability, e.g., when the wheel eccentricity value changes from 1 µm to 3 µm. The eccentric rotation deviation of the grinding wheel should be minimized to less than 3 µm, which is the upper limit value of stable grinding, or should even be 'eliminated' prior to grinding with a dressing or reconditioning technique, as well as by use of dynamic balancer with the aid of some specific devices.

Nomenclatures

a_p	total cutting depth of grinding process, [µm]
B_i	width of abrasive grit geometry in contact zone, [µm]
d_s	grinding wheel diameter, [mm]
f_t	feed rate per revolution of grinding wheel, [µm]
h_r	total normal cutting depth of continuously active grits simultaneously removing material in contact zone, [µm]
$h_r(\varphi_i)$	incremental cutting depth of a single active abrasive grit in contact zone, [µm]
$h_g(\varphi_i)$	theoretical cutting depth of a single active abrasive grit, [µm]
$\Delta h(\varphi_i)$	normal cutting depth with eccentrically rotational deviation, [µm]
$h_w(\varphi_i)$	local amplitude of peak-point on initial surface waviness of workpiece, [µm]
k	sampling times within full length of workpiece surface
k_n	sampling times in each sampling zone
L	sample length on the machined surface, [mm]
l_p	length of a single scratch groove, [µm]
m	number of active abrasive grits simultaneously working in contact zone in peripheral direction, [grits/mm²]
$OXYZ$	grinding kinematics coordinate system of machine tool
$O'X'Y'Z'$	grinding kinematics coordinate system of abrasive wheel
$O''X''Y''Z''$	local kinematics coordinate system of working grit in contact zone
R_a	surface roughness of workpiece machined, [µm]
$R_{a,wx}$	average longitudinal height between peak-points and valley-points in local surface topography, [µm]
$R_w(t)$	rotatory radius of adjacent abrasive grits at the instant time t, , [µm]
$R_w(t–T)$	rotatory radius of adjacent abrasive grits at the previous time $t–T$, [µm]
R_{si}	rotatory radius of active abrasive grit i around machine tool spindle center, [µm]
S_j	section area of one groove formed by single abrasive grit with some type of geometry, [µm²]
S_n	full section area of grooves formed by all abrasive grits with three types of geometries, [µm²]
T	discrete time interval between current and adjacent working grits, [s]
v_s	peripheral speed of grinding wheel, [m/s]
v_w	feed speed of workpiece, [m/s]
V_w	incremental volume of instantaneously removed material, [mm³]
W_{nj}	proportion of numbers of active grits with different types of geometries, [%]
y_a	average longitudinal height between points of peak and valley along peripheral direction, [µm]
δ_e	wheel eccentricity value, [µm]
σ	standard deviation of protrusion heights of abrasive grits, [µm]
ϕ	effective included angle of current abrasive grit, [°]
Φ_i	phase difference of motion trajectory of adjacent abrasive grits in peripheral direction, [°]
φ_{e0}	initial position angle of abrasive wheel, [°]
φ_e	relative position angle with actual wheel rotational center, [°]
φ_i	rotatory position angle of the grit i, [°]
ω	angular velocity of abrasive wheel, [rad/s]
θ	rotational angle of spindle of abrasive wheel, [°]
θ_s	rotation included angle from machine tool spindle center to eccentrically rotational center of abrasive wheel, [°]

λ_s average distance between adjacent active abrasive grits on surface of grinding wheel, [μm]
Ω entire included angle of grit in interaction zone, [°]
ψ phase difference between previous and current waviness trajectory, [rad]
Λ_{si} protrusion height of abrasive grit *i* from surface of wheel, [μm]
Λ_{savg} mean protrusion height of abrasive grit *i* from surface of wheel, [μm]

References

[1] Zhang, Y.Z., Fang, C.F., Huang, G.Q, Xu, X.P. Modeling and simulation of the distribution of undeformed chip thickness in surface grinding. *Int J Mach Tools Manuf* 127 14-27 (2018) **DOI:10.1016/j.ijmachtools.2018.01.002**.

[2] Darafon, D., Warkentin, A., Bauer, R. 3D metal removal simulation to determine uncut chip thickness, contact length and surface finish in grinding. *Int J Adv Manuf Technol* 66 1715-1724 (2013) **DOI:10.1007/s00170-012-4452-1**.

[3] Rasim, M., Mattfeld, P., Klocke, F. Analysis of the grit shape influence on the chip formation in grinding. *J Mater Process Technol* 226 60-68 (2015) **DOI:10.1016/j.jmatprotec.2015.06.041**.

[4] Tian, L., Fu, Y.C., Li, H.Y., Ding, W.F. The influence of speed on material removal mechanism in high speed grinding with single grit. *Int J Mach Tools Manuf* 89 192-201 (2015) **DOI:10.1016/j.ijmachtools.2014.11.010**.

[5] Yang, X. X., Zhang, B., Bai, Q., Kang, R.K., Tang, J.G. Effect of grit size on subsurface characterization of pure iron subjected to the orthogonal cutting. *Int J Adv Manuf Technol* 120 5793-5806 (2022) **DOI:10.1007/s00170-022-09156-6**.

[6] Axinte, D., Butler-Smith, P., Akgun, C. On the influence of single grit micro-geometry on grinding behavior of ductile and brittle materials. *Int J Mach Tools Manuf* 74 12-18 (2013) **DOI:10.1016/j.ijmachtools.2013.06.002**.

[7] Zagórski, I., Kulisz, M., Szczepaniak, A. Roughness parameters with statistical analysis and modelling using artificial neural networks after finish milling of magnesium alloys with different edge helix angle tools. *Stroj Vestn-J Mech Eng* 70 27-41 (2024) **DOI:10.5545/sv-jme.2023. 596**.

[8] Li, C., Piao, Y.C., Meng, B.B., Hu, Y.X, Li, L.Q., Zhang, F.H. Phase transition and plastic deformation mechanisms induced by self-rotating grinding of GaN single crystals. *Int J Mach Tools Manuf* 172 1-15 (2022) **DOI:10.1016/j.ijmachtools.2021.103827**.

[9] Wang, X.Z., Liu, Q.Y., Zheng, Y.H., Xing, W., Wang, M.H. A grinding force prediction model with random distribution of abrasive grits: considering material removal and undeformed chips. *Int J Adv Manuf Technol* 120 7129-7233 (2022) **DOI:10.1007/s00170-022-09213-0**.

[10] Zhu, H., Ge, S.R., Huang, X.L., Zhang, D., Liu, J.L. Experimental study on the characterization of worn surface topography with characteristic roughness parameter. *Wear* 255 309-314 (2003) **DOI:10.1016/S0043-1648(03)00215-1**.

[11] Santhosh, D.K., Pušavec, F., Krajnik, P. Grinding of cemented carbide using a vitrified diamond pin and lubricated liquid carbon dioxide. *Stroj vestn-J Mech Eng* 69 435-443 (2023) **DOI:10.5545/sv-jme.2023.658**.

[12] Zou, L., Li, H., Wang, W.X., Huang, Y., Li, Y.T. A precision grinding technology for zirconium alloy tubes based on ultrasonic wall thickness automatic measurement system. *Int J Adv Manuf Technol* 121 323-335 (2022) **DOI:10.1007/s00170-022-09314-w**.

[13] Duan, N., Yu, Y.Q., Wang, W.S., Xu, X.P. Analysis of grit interference mechanism for the double scratching of monolayer silicon carbide by coupling the FEM and SPH. *Int J Mach Tools Manuf* 120 49-61 (2017) **DOI:10.1016/j.ijmachtools.2017.04.012**.

[14] Hu, Z.W., Chen, Y., Lai, Z.Y., Yu, Y.Q., Xu, X.P. Coupling of double grains enforces the grinding process in vibration-assisted scratch: Insights from molecular dynamics. *J Mater Process Technol* 304 1-14 (2022) **DOI:10.1016/j.jmatprotec.2022.117551**.

[15] Guo, X., Zhai, C., Kang, R. The mechanical properties of the scratched surface for silica glass by molecular dynamics simulation. *J Non-Cryst Solids* 420 1-6 (2015) **DOI:10.1016/j.jnon-crysol.2015.04.001**.

[16] Zagórski, I. Surface roughness evaluation of AZ31B magnesium alloy after rough milling using tools with different geometries. *Stroj Vestn-J Mech Eng* 70 355-368 (2024) **DOI:10.5545/sv-jme. 2023.885**.

[17] Jia, X.F., Wang, H., Zhao, F. Critical grinding depth of ultrasonic vibration-assisted electrolytic in-process dressing grinding in ZTA ceramics. *Int J Adv Manuf Technol* 120 7127-7141 (2022) **DOI:10.1007/s00170-022-09066-7**.

[18] Chen, Y., Jiang, C., Chen, X., Huang, G.Q., Hu, Z.Y. Study on the dynamic influence of the distribution of cutting depth on the ground surface quality in a precision grinding process. *J Manuf Process* 107 134-143 (2023) **DOI:10.1016/j.jmapro.2023.10.028**.

[19] Zhang, S.J., Yu, J.J., Tu, S., Xiong, Z.W. A theoretical and experimental study of spindle imbalance induced forced vibration and its effect on surface generation in diamond turning. *Int J Mach Tools Manuf* 133 61-71 (2018) **DOI:10.1016/j.ijmachtools.2018.06.002**.

[20] Zhang, B., Uematsu, T. Surface generation mechanism in helical scan grinding: An analytical study. *J Mater Process Technol* 91 206-214 (1999) **DOI:10.1016/S0924-0136(98)00415-4**.

[21] Song, T.J., Zhou, Z.X., Li, W., Huang, X.M., Chen, Q.D. Roughness model for helical flute of cemented carbide end milling under grinding. *J Mech Eng* 53 185-192 (2017) **DOI:10.3901/JME.2017.17.185**.

[22] Chen, Y., Chen, X., Hu, Z.W., Duan, N. Comprehensive influence of ultrasonic vibration-assisted technology on material removal mechanism under the excitation of regenerative vibration in precision grinding process. *Int J Adv Manuf Technol* 129 3645- 3657 (2023) **DOI:10.1007/s00170-023-12571-y**.

[23] ANSI-B74.16:2002. American national standard: procedure for bulk density of abrasive grains. American national standards institute (2002) New York.

Acknowledgement *This work is supported by the Natural Science Basic Research General Program of Shaanxi Province (Grant No 2024JC-YBMS-428). The authors would like to thank Ph.D. Kathleen League of DePaul University of Chicago and Prof. Bill Martin of University of Kansas from the United States for proofreading & editing.*

Received: 2025-05-13, revised: 2025-08-03, accepted: 2025-09-22
as Original Scientific Paper.

Data Availability *The data that underpin the results of this research are available for use by other researchers. Additionally, the corresponding author can provide additional raw data upon reasonable request.*

Author Contribution *Yizun Chen: Methodology, Formal analysis, Validation, Writing - original draft; Yu Sun: Methodology, Supervision, Project Administration, Writing - review & editing. All authors have contributed significantly to this work and thoroughly reviewed and approved the final version of the manuscript.*

Teoretična in eksperimentalna raziskava mikroskopske tvorbe površine pri preciznem brušenju z diskretno metodo

Povzetek *Topografija površine obdelovanca, ustvarjena pri preciznem brušenju, je odvisna ne le od ključnih procesnih parametrov, temveč tudi od porazdelitvenih značilnosti aktivnih abrazivnih zrn na površini brusnega kolesa, vključno s številom aktivnih zrn v kontaktni coni, njihovo morfologijo in globino reza posameznega zrna v normalni smeri. Pri majhnih globinah reza (manj kot 5 μm) in majhnih ekscentričnih rotacijah brusnega kolesa (manj kot 3 μm) se vplivi prvotne topografije površine obdelovanca ter dinamične globine reza abrazivnih zrn pogosto zanemarjajo pri proučevanju mikroskopske tvorbe površine. V tem članku je uporabljena diskretna metoda (DM) za razvoj teoretičnega kinematičnega modela za napoved topografije obdelane površine. Primerjava med izmerjenimi in simuliranimi vrednostmi značilnosti topografije (prask) je pokazala, da izboljšani napovedni model topografije površine dobro zajame vplive začetne površinske topografije, ekscentričnega vrtenja brusnega kolesa ter prekrivanja prask pri kompleksnih procesnih pogojih, z napako napovedi približno 10 %. V primerjavi z dvema pogosto uporabljenima empiričnima enačbama se natančnost napovedi modela DM za topografijo obdelane površine izboljša za 20 %. Pri izračunu volumna odstranjenega materiala se natančnost napovedi inkrementalnega volumskega modela odstranitve materiala poveča za približno 9 % do 19 % v primerjavi z rezultati napovedi, ki kot ključno spremenljivko upoštevajo celotno presečno površino aktivnega zrna.*

Ključne besede *precizno brušenje, mikroskopska topografija površine, globina reza, diskretna metoda (DM), hrapavost površine*